1-1-2018

Microscopic origin of highly enhanced supercurrent in 122 pnictide superconductor

Jincheng Zhuang
University of Wollongong, jincheng@uow.edu.au

Wai Kong Yeoh
University of Sydney, University of Wollongong, wyeoh@uow.edu.au

H W. Yen
University of Sydney

Xun Xu
University of Wollongong, xun@uow.edu.au

Yi Du
University of Wollongong, ydu@uow.edu.au

See next page for additional authors

Microscopic origin of highly enhanced supercurrent in 122 pnictide superconductor

Abstract

By a combination of microstructure analysis techniques, we reveal the structural origin of the extremely high supercurrent (up to the practical level of 0.1 MA/cm 2 at 10 T, 4.2 K) in Sr 0.6 K 0.4 Fe 2 As 2 (122) tape. Transmission Kikuchi diffraction analysis reveals that hot pressing promotes a very high fraction of low-angle grain boundaries and texturing of the crystals, which is beneficial for the intergrain physical properties. Moreover, the unique characteristics of low-angle grain boundaries favor both long-range dislocations and short-range dislocations that totally change the pinning mechanism of the bulk 122 system. These defects combined with the grain texturing are not only effective for pinning vortices in the superconducting state, but also improve inter-granular supercurrent degradation, leading to substantially enhanced supercurrent over a wide range of magnetic fields.

Disciplines

Engineering | Physical Sciences and Mathematics

Publication Details

Zhuang, J., Yeoh, W., Yen, H., Xu, X., Du, Y., Liu, H., Yao, C., Ma, Y., Wang, X., Ringer, S. & Dou, S. (2018). Microscopic origin of highly enhanced supercurrent in 122 pnictide superconductor. Journal of Alloys and Compounds, 754 1-6.

Authors

Jincheng Zhuang, Wai Kong Yeoh, H W. Yen, Xun Xu, Yi Du, H Liu, Chao Yao, Yanwei Ma, Xiaolin Wang, Simon Peter Ringer, and Shi Xue Dou

Journal of Alloys and Compounds 754 (2018) 1–6

Contents lists available at ScienceDirect

Journal of Alloys and Compounds

journal homepage: http://www.elsevier.com/locate/jalcom

Microscopic origin of highly enhanced supercurrent in 122 pnictide superconductor

J.C. Zhuang [a], W.K. Yeoh [a, b, c, *], H.W. Yen [d], X. Xu [a], Y. Du [a], H.W. Liu [c], C. Yao [e], Y.W. Ma [e], X.L. Wang [a], S.P. Ringer [b], S.X. Dou [a]

[a] Institute for Superconducting and Electronic Materials, University of Wollongong, Wollongong, New South Wales 2500, Australia
[b] School of Aerospace, Mechanical and Mechatronic Engineering, University of Sydney, Sydney, New South Wales 2006, Australia
[c] Australian Centre for Microscopy & Microanalysis University of Sydney, Sydney, New South Wales 2006, Australia
[d] Department of Materials Science & Engineering, National Taiwan University, Taipei, People's Republic of China
[e] Key Laboratory of Applied Superconductivity Institute of Electrical Engineering, Chinese Academy of Sciences, Beijing 100190, People's Republic of China

ARTICLE INFO

Article history:
Received 17 January 2018
Received in revised form
24 April 2018
Accepted 25 April 2018
Available online 26 April 2018

Keywords:
Grain boundaries
Supercurrent
Weak-link
Iron-based superconductors

ABSTRACT

By a combination of microstructure analysis techniques, we reveal the structural origin of the extremely high supercurrent (up to the practical level of 0.1 MA/cm^2 at 10 T, 4.2 K) in $Sr_{0.6}K_{0.4}Fe_2As_2$ (122) tape. Transmission Kikuchi diffraction analysis reveals that hot pressing promotes a very high fraction of low-angle grain boundaries and texturing of the crystals, which is beneficial for the intergrain physical properties. Moreover, the unique characteristics of low-angle grain boundaries favor both long-range dislocations and short-range dislocations that totally change the pinning mechanism of the bulk 122 system. These defects combined with the grain texturing are not only effective for pinning vortices in the superconducting state, but also improve inter-granular supercurrent degradation, leading to substantially enhanced supercurrent over a wide range of magnetic fields.

1. Introduction

The competitive advantage of superconducting materials is the ability to carry high current, thus generating strong magnetic fields in significant volumes. Due to the small size of a single crystal, the superconductors used for applications are polycrystalline wires or tapes, where many grain boundaries (GBs) are inevitable. The GBs coexist with the superconducting matrix in the form of a network, across which, long-range supercurrent has to pass, evoking the importance of GB superconducting properties. It is universally found that the critical current density, J_c, is proportional to the density of GBs for type-I low temperature superconductors, such as Nb-Ti, $SnMo_6S_8$, and MgB_2 [1–4]. In this type of superconductor, GBs are not intrinsic barriers to supercurrent flow, and the low binding energy of vortices to GBs leads to the enhancement of vortex pinning capacity [5–7]. Nevertheless, type-II high temperature superconductors, which are expected to have a larger application market, suffer from obvious weak-link behaviour of GBs. The weak-link behaviour is caused by the quasi-two-dimensional (2D) phase, which produces weak growth texture, with almost randomly distributed values of the GB misorientation angle, θ. The GB critical current density ($J_{cgb}(\theta)$) falls off exponentially when the GB misorientation angle θ exceeds the critical angle θ_c, which has a value of 3–5° [8,9]. Recently, in the newly discovered iron-based superconductors (IBSs), in the $BaFe_2As_2$-122 system and the Fe(Se,Te)-11 system, the value of θ_c could be improved up to 9°, making IBSs more promising materials for application in high J_c superconducting tapes [10,11]. Since high J_c of more than 1 MA/cm [2] has been reported in single crystal and epitaxial thin films of IBSs, the next step is achieving special grain-to-grain low-angle misorientation and improving the texture of the whole sample [12–15]. In a recent breakthrough, transport J_c at a practical level (0.1 MA/cm^2) at 4.2 K and 10 T was realized by the improvement of *c*-axis textured superconducting tape [15,16]. Detailed analysis of the microstructure to reveal the origin of the high J_c is still ambiguous, however.

In this work, we carried out transmission Kikuchi diffraction (TKD) using a Zeiss Auriga scanning electron microscope to quantitatively describe the crystal phase formed at each point of the micrograph with high resolution. It was found that special GBs with

* Corresponding author. Institute for Superconducting and Electronic Materials, University of Wollongong, Wollongong, New South Wales 2500, Australia.
E-mail address: waikong.yeoh@sydney.edu.au (W.K. Yeoh).

https://doi.org/10.1016/j.jallcom.2018.04.281
0925-8388/

low angle misorientation combined with high texture along the *c*-axis are promoted by using the hot pressing (HP) method. Transmission electron microscopy (TEM) with weak beam dark field (WBDF) images reveals that both long-range dislocations and short-range dislocations are assembled in low-angle GBs, which totally change the pinning mechanism of the bulk 122 system. Textured crystal structure, special low-angle GBs, and a high density of defects are leading to the improvement of supercurrent to a practical level over a wide range of magnetic fields.

2. Experimental section

Preparation of Sr-122 tape: Ag-clad $Sr_{0.6}K_{0.4}Fe_2As_2$ tapes containing Sn as an additive were fabricated by the *ex-situ* powder-in-tube (PIT) method. Sr filings, K pieces, and Fe and As powders in the ratio of Sr: K: Fe: As = 0.6: 0.5: 2: 2.05 were mixed for 12 h by the ball-milling method. The milled powders were packed into Nb tubes and then sintered at 900 °C for 35 h. The as-prepared Sr-122 superconducting precursors were then ground into powders under Ar atmosphere. In order to increase the grain connectivity, the precursors were mixed with 5 wt% Sn by hand with an agate mortar. Then, the fine powders were packed into Ag tubes with outer diameter (OD) of 8 mm and inner diameter (ID) of 5 mm. These tubes were sealed and then cold worked into tapes (~0.4 mm thickness) by swaging, drawing, and flat rolling. Finally, hot pressing was performed on the 60 mm long tapes under ~30 MPa at the sintering temperature of 850 °C for 30 min. More detailed information on the fabrication can be found elsewhere [16,19].

Superconducting properties measurements and microstructure characterization of Sr-122 tape: Transport and magnetization measurements under different magnetic fields were carried out on a 14 T physical properties measurement system (PPMS). The transmission Kikuchi diffraction was carried out using a Zeiss Auriga scanning electron microscope, which enabled us to quantitatively describe the crystal phase formed at each point of the micrograph with a minimum resolution of about 1 nm. The orientation of the crystals at each point was determined by using a HKL Nordlys 2 system. Electron microscopy studies were carried out using a JEOL 2200FS instrument equipped with electron energy loss spectroscopy, with a 200 kV field emission gun and an in-column omega type energy filter.

3. Results and discussion

3.1. Superconducting properties of HP Sr-122 tape

Fig. 1(a) displays the comparative results of investigations of the magnetic field dependence of transport J_c at 4.2 K for tapes or wires fabricated by different methods. The $(Sr,K)Fe_2As_2$ wires produced by the simple rolling technique exhibit the lowest J_c (less than 10^4 A/cm^2) among all the results [17]. The value of J_c was improved up to more than 10^4 A/cm^2 by cold pressing with enhanced pressure in tape samples [17]. For the wires synthesised by cold isostatic pressure combined with a hot isostatic pressure process, the self-field J_c reached as high as 0.1 MA/cm^2, which is a criterion for practical application [18]. J_c shows a rapid decrease in low field, however, reflecting the typical weak-link behaviour between GBs [11]. Such a dip could be related to the large GB misorientation induced by randomly distributed grains and the FeAs wetting phase formed in the GBs, both of which decrease the J_c in GBs [18]. J_c of 0.1 MA/cm^2 at 10 T has been realized in hot pressed tapes with high density and *c*-axis orientation [19]. It should be noted that this is the first time that J_c of IBS tapes has reached the practical level of 0.1 MA/cm^2 at 10 T. Another significant phenomenon is that J_c shows almost field independence in the measured field range, indicating strong pinning in the tape. Fig. 1(b) shows the temperature dependence of the upper critical field, B_{c2}, for both $B//ab$ and $B//c$. A small anisotropy is calculated by using $\gamma = B_{c2}^{B//ab}/B_{c2}^{B//c}$ ~1.5, which is comparable to the value for 122 single crystals, but larger than that for polycrystalline samples (~1) [20], indicating that the tape has textured structure. Moreover, the smaller anisotropy value compared to those of other Fe-based superconductors (>3) is suitable for potential magnetic applications.

3.2. Grain orientation map of HP Sr-122 tape

The transmission Kikuchi diffraction (TKD) technique is used to analyse the distribution of grain orientations. Fig. 2(a)-(c) provides examples of microstructure, band contrast, and inverse pole figure images derived from the TKD map after noise removal, respectively. The grain size variation is huge, from 2 μm down to as small as 10 nm. Nevertheless, the smaller grains are the dominant group, with average grain size of 200 nm, which is similar to the findings of a previous report on Ba-122 wires [18]. There is a strong correspondence between the different coloured regions (representing different orientations) in the inverse pole figures and the band contrast image.

The angles of GB misorientation are classified into three types: high-angle GBs with ≥ 10° misorientation with respect to adjacent grains are denoted by the red lines; low-angle GBs denoted by the green lines exhibit only 2–10° misorientation; and super low-angle GBs denoted by grey lines show very low (<2°) misorientation. A quantitative analysis reveals that around 66% of grains have misorientation angles below 15°. Furthermore, nearly half of the GBs possess misorientation angles less than the critical angle θ_c (9°) in iron-based superconductors. Since these GBs (misorientation

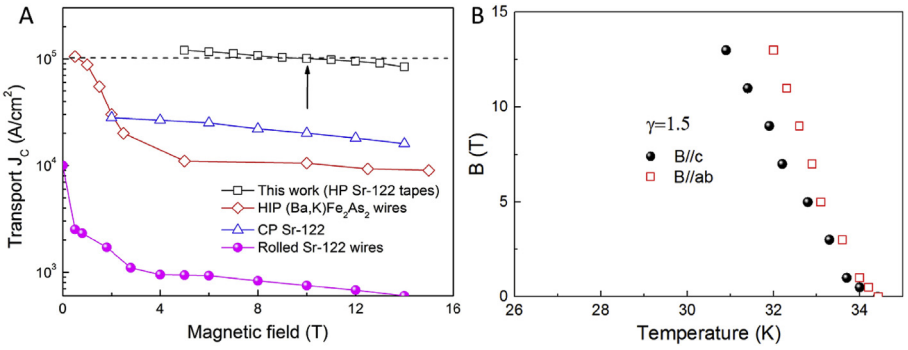

Fig. 1. (a) Comparative study of transport J_c as a function of magnetic field at 4.2 K for tapes or wires fabricated by different methods [17–19]. The black arrow points at the criterion for practical application. (b) Temperature dependence of the upper critical field B_{c2} for both $B//ab$ and $B//c$.

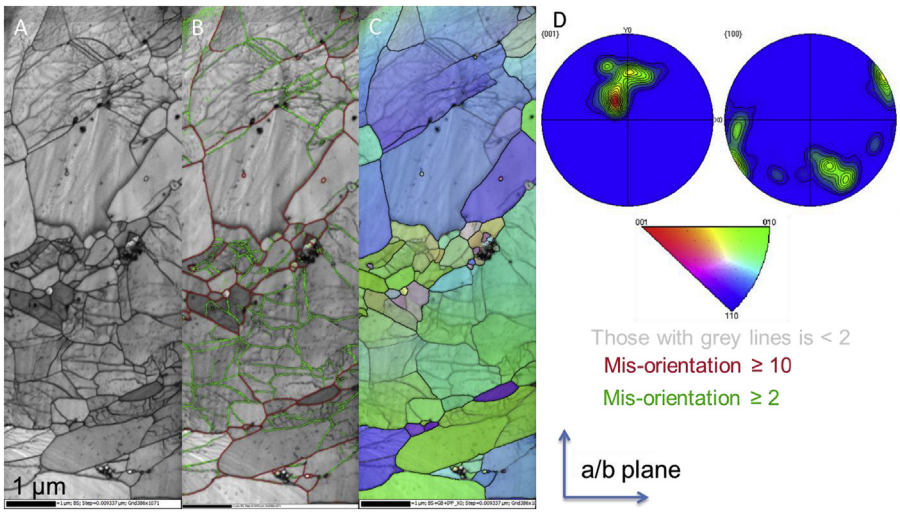

Fig. 2. (a)–(c) Microstructure, band contrast, and inverse pole figure images derived from the TKD map after noise removal, respectively. (d) The degree of preferred orientation in the {001} and {100} pole figures along the x_0 and y_0 directions.

angle $\leq 9^\circ$) show almost the same J_{cgb} as the intragrain J_c, the low-angle GBs and super low-angle GBs could be treated as "special" GBs. Such a high value for the fraction of "special" GBs means that a "special" GB network could form, which would favour the passage of current, improving the connectivity and inter-grain J_c of the whole sample. Fig. 2(d) displays the degree of preferred orientation in the {001} and the {100} pole figures along the x_0 and y_0 directions. There is only one preferred orientation in the intensity distribution of the {001} pole figure, suggesting a high *c*-axis textured structure in the tape. Although the intensity distribution in the {100} pole figure does not exhibit the fourfold symmetry observed in the pole figures of thin films [21], three preferred orientations could be identified, indicating alignment in the *ab* plane rather than the randomly distributed grains found in the polycrystalline samples. All these results imply that the hot pressing technique not only promotes low-angle GBs, but also constrains the grain growth of the sample to specific orientations in both the *c*-axis direction and the *ab* plane.

3.3. Microstructure characterization of low-angle grain boundaries and dislocations crossing the grain boundaries

To find the microstructure of GBs, we conducted a high-resolution transmission electron microscope (HRTEM) investigation of the GBs between nanocrystals, as shown in Fig. 3(a). Two grains with different orientations are mapped in the microscope image, which is confirmed by the fast Fourier transform (FFT) patterns, as shown in Fig. 3(b) and (d), respectively, corresponding to the areas connected by red arrows in Fig. 3(a). A clean boundary without a secondary impurity phase is observed in the GB labelled by the green line in Fig. 3(a). In order to make a quantitative analysis of the value of the GB angle, the indexed results for the two FFT images have been plotted in Fig. 3(c) and (e), respectively. By simulating the diffraction pattern for the tetragonal structure of $SrFe_2As_2$ crystal, it was found that the two grains are very close to [001] orientation. The grain on the left has the [001] orientation and the grain on the right is in the [027] direction. The [027] direction could be obtained by tilting the [001] direction along the (020) plane by about 5°. Fig. 3(h) displays the inverse FFT image of the GB marked by the red square in Fig. 3(a) to show the dislocation array at this low-angle tilt boundary. It can be seen clearly that the low-angle GB is comprised of an array of dislocations, which is marked by the red circles, and channels of slightly distorted crystal. It is well known that the low-angle GBs with $\theta < 10^\circ$ are treated as a simple system because the GB dislocation spacing D is given by the Frank formula $D = (b/2)/\sin(\theta/2)$, where b is the norm of the corresponding Burgers vector [22,23]. Taking the lattice constant $c = 1.26$ nm for the $SrFe_2As_2$ sample into account [24,25], the dislocation spacing D is estimated to be around 1.44 nm, which is in agreement with the experimental distance (~1.46 nm) in Fig. 3(h). This validates the small θ between the two grains obtained from the TEM results. In general, a GB is mainly composed of distorted nanocrystals, and the closure of the channel by the distorted crystals is regarded as the onset of weak-link behavior [26]. In the current study, clean low-angle GBs without impurity phase are friendly to the current flow.

Fig. 4 (a), (c), and (d) displays TEM images for different grains in the hot-pressed tape. Notably, there are a high density of dislocations and dislocation lines, labelled by white arrows, which are distributed in all three grains. All these dislocations have sizes on the nanometer scale, giving rise to almost perfect pinning centres for iron-based superconductors [12,27]. The weak beam dark field (WBDF) technique is used to provide a clear view of the distribution of these dislocations. Fig. 4(b) is the WBDF image of the grain measured in Fig. 4(a). Interestingly, due to the well-developed texture and small misorientation, as revealed by the TKD results in Fig. 2, the dislocation lines penetrate through the GB, improving the interaction of the vortices in the GBs with the pinned vortices in the grains (Abrikosov vortices). The GB and adjacent two grains in superconductors act as a Josephson junction. The vortices could be pinned by the dislocations in low-angle GBs, which are denoted as Josephson vortices [23]. When current flows through the GBs, the vortices form in the direction parallel to the GB. Such vortices flow much more easily than the Abrikosov vortices, however, reflecting the result that J_{cgb} is always smaller than the intragrain J_c. The highly dense dislocation lines are made up of nanosized defects elongated along the direction perpendicular to the GB, pinning the vortices parallel to the GB in a single-vortex model, even in high magnetic field with a small spacing of vortices [27]. In this case, a high barrier is induced by enhanced Abrikosov-Josephson vortex hybridization to prevent the flux of GB vortices. The power-law dependence of $J_c(B)$ up to 14 T without a magnetic granularity transition in Fig. 1 is strong evidence for the improved grain vortex – GB vortex interaction [28].

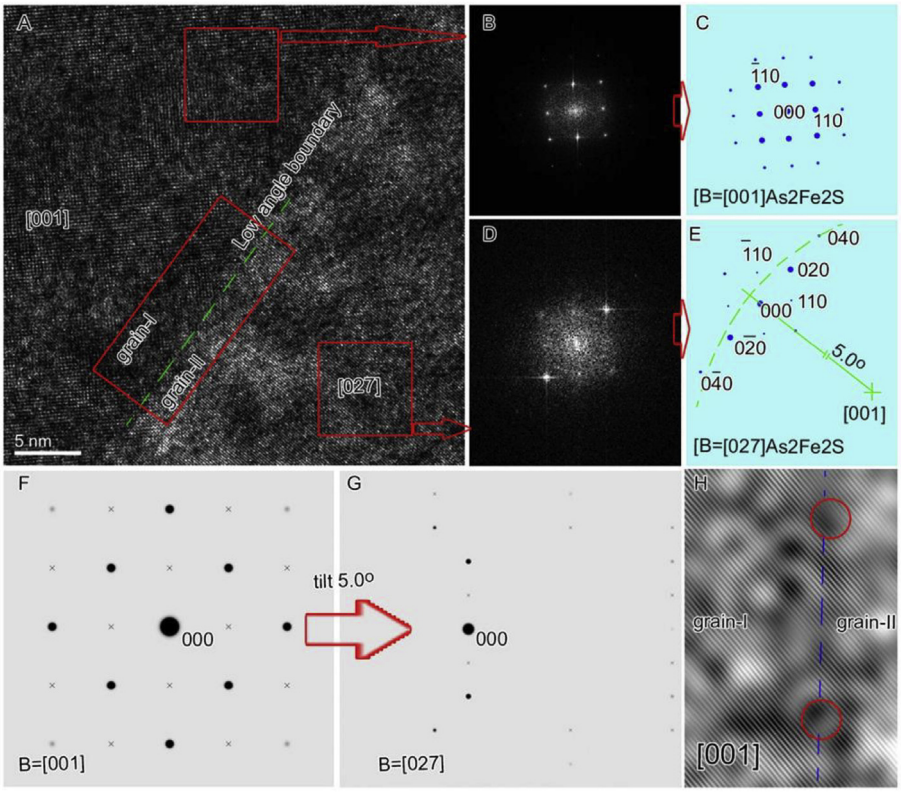

Fig. 3. TEM investigations of grain boundaries between $SrFe_2As_2$ nanocrystals by means of HRTEM imaging. (a) HRTEM image showing the low angle boundary between two adjacent grains, both of which are used for generating fast Fourier transform (FFT) patterns from the areas marked by the corresponding red squares, in order to reveal the crystal orientation. (b) and (d) are the FFT patterns corresponding to the areas connected by arrows in panel A. (c) and (e) are the indexed results for the FFT patterns in panel (b) and panel (d), respectively. (f) and (g) Simulated electron diffraction patterns of $SrFe_2As_2$ for the [001] direction and the [027] direction, respectively. (h) Inverse FFT image generated by the (110) plane to show the dislocation array at this low-angle tilt boundary. (For interpretation of the references to colour in this figure legend, the reader is referred to the Web version of this article.)

3.4. Pinning mechanisms of grain boundaries and dislocations

It is important to explore the role of dislocations in both GBs and grains in the pinning mechanism for the enhancement of J_c. All these defects produce strains and change the local doping level as well as the structural parameters, such as the bond angle in tetragonal structures, suppressing superconductivity at distances on the order of a few Burgers vectors [29]. According to the phase diagram of the K doped 122 system, the K composition $x = 0.4$ is the optimal doping level [30]. Thus, the dislocation cores in our sample could be either superconducting phase with low superconducting critical temperature, T_c, or non-superconducting phase. Either the dislocation cores or lattice strain could induce the shift of the chemical potential by a value of around 100 meV for a θ ~9° GB [23]. This shift is much larger than the range of Fermi energies, $E_F = 25–50$ meV in the 122 system, making the GB non-superconducting or insulating [31]. The scaling behaviour of J_c in both the $B//ab$ and the $B//c$ directions was investigated to understand the pinning mechanism of these dislocations. The critical current densities are scaled by following the theoretical approach proposed by Griessen et al. [32] In the case of δl pinning, evoked by the spatial fluctuation of the charge-carrier mean free path, l, the normalized critical current density can be described as:

$$J_c(t)/J_c(0) = (1 - t^2)^{5/2}(1 + t^2)^{-1/2} \quad (1)$$

while for the δT_c pinning associated with the spatial fluctuation of the Ginzburg parameter caused by the variation of the T_c, it is

$$J_c(t)/J_c(0) = (1 - t^2)^{7/6}(1 + t^2)^{5/6} \quad (2)$$

where $t = T/T_c$. Fig. 5 shows the normalized $J_c(t)$ for both $B//ab$ and $B//c$, along with the theoretical curves for the scenarios of δl pinning and δT_c pinning. A remarkable agreement between the normalized results and the theoretical δl pinning fitting results, demonstrating that the dominant pinning in this sample is δl pinning, which is associated with spatial fluctuation of the charge-carrier mean free path.

According to the Dew-Hughes model, δl pinning is evoked by non-superconducting particles with diameters larger than the superconducting coherence length, ξ, that are embedded in the superconducting matrix [33]. It should be noted, in K-doped 122 with similar composition and underdoped single crystals, competition between antiferromagnetism (AFM) and superconductivity (SC) results in the coexistence of δl pinning and δT_c pinning. Therefore, the dominant δl pinning in our tape is likely due to the non-superconducting phase defects such as dislocations or the low-angle GBs [34]. A similar phenomenon has been observed in J_c enhancement by irradiation, where the pinning mechanism changes from δT_c pinning to δl pinning after introducing non-superconducting defects [35]. Research on the effects of the doping level on the pinning mechanism shows that stronger pinning and higher critical current densities emerge in an underdoped sample, in which the pinning centres originate from non-superconducting defects, such as orthorhombic/antiferromagnetic domains [36]. These investigations imply that non-superconducting defects could be more effective pinning centres

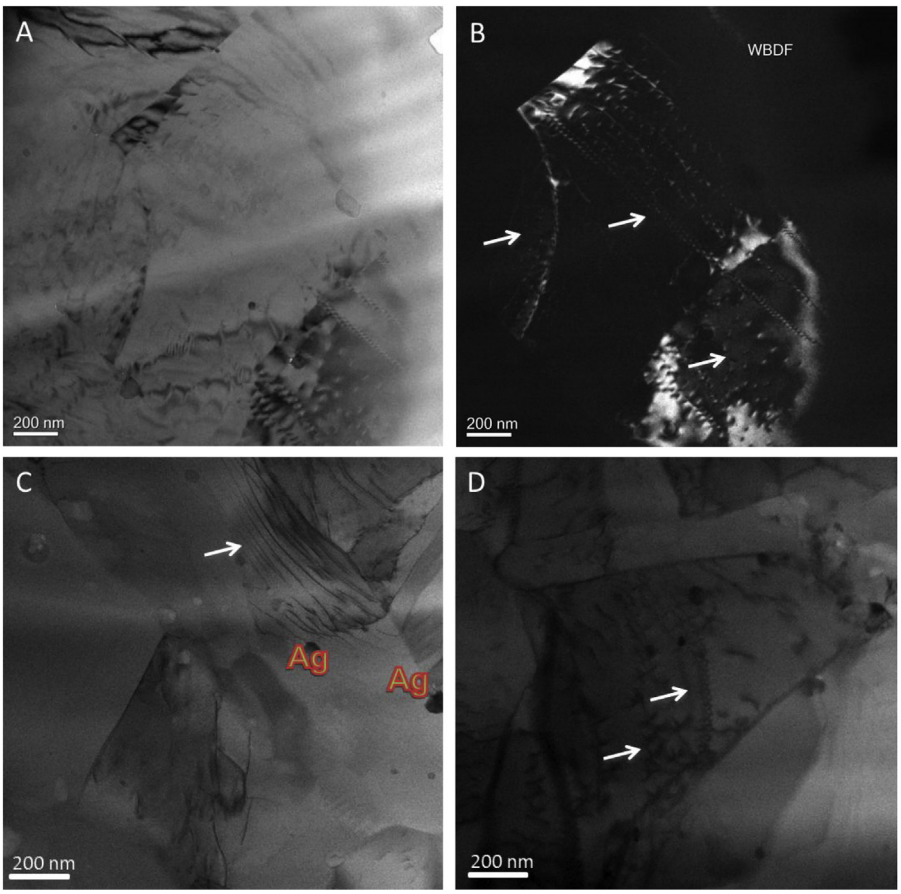

Fig. 4. (a), (c), and (d) TEM images of different grains in the hot pressed tape. White arrows are used to label the dislocations and dislocation lines. (b) WBDF image of the grain shown in panel (a).

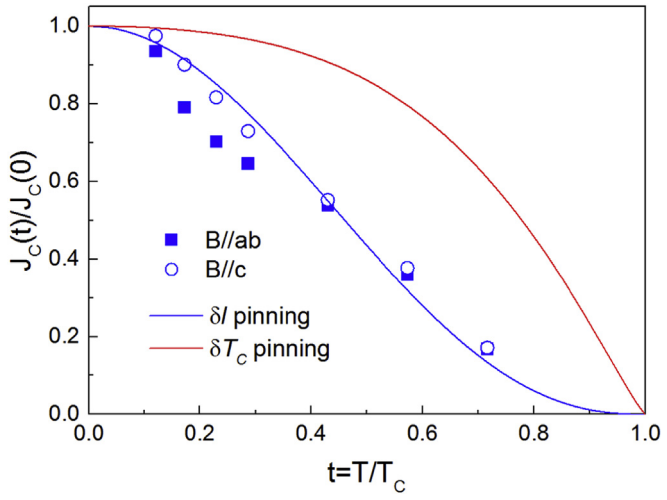

Fig. 5. Normalized critical current density as a function of reduced t for both $B//ab$ and $B//c$. The red line and blue line represent the theoretical curves expected in the cases of δT_c pinning and δl pinning, respectively. (For interpretation of the references to colour in this figure legend, the reader is referred to the Web version of this article.)

compared with δT_c pinning centres. It has been reported that the critical value of the effective pinning fraction is around 10%, above which, the pinning force starts to decrease due to the current blocking effect of defects [37]. The concentration of defects is much smaller than the critical value, as can be viewed from Fig. 3, so the J_c of our tape could be further increased with more pinning centres by an optimised GB engineering technique. It should be noted that nematic fluctuations in K-doped 122 system show the strong dependence on the concentration of K, which may affect the pinning mechanism [38,39]. Nevertheless, the nematic fluctuations disappear in the optical K-doped case ($Sr_{0.6}K_{0.4}Fe_2As_2$) [39], which is expected to make negligible effect on the pinning mechanism.

4. Conclusion

In summary, the practical level of J_c is realized in a $Sr_{0.6}K_{0.4}Fe_2As_2$ (122) tape produced by the hot pressing technique. The GB engineering process facilitates textured crystal structure along the c-axis direction and a high ratio of special GBs, improving the intergrain connectivity. A high density of dislocations was formed in the grains, and dislocation lines crossed the GBs in our tape, enhancing the coupling between grains and preventing the degradation of J_c in high magnetic field. Our investigation of the pinning mechanism implies that primary dislocations and dislocation lines are non-superconducting phase, acting as δl pinning centres and effectively increasing J_c. Our work presents an effective way to further improve pinning strength and critical current density by introducing more effective defects by GB engineering techniques.

Acknowledgements

The authors thank Dr Tania Silver for critical reading of the

manuscript. We thank P. W. Trimby for technical help on transmission Kikuchi diffraction. This work is financially supported by an Australian Research Council Discovery Project (DP140102581, DP160102627) and Linkage Infrastructure, Equipment and Facilities grants (LE100100081, LE110100099). The authors acknowledge scientific and technical support from the Australian Microscopy and Microanalysis Research Facility (AMMRF) at The University of Sydney.

Appendix A. Supplementary data

Supplementary data related to this article can be found at https://doi.org/10.1016/j.jallcom.2018.04.281.

References

[1] D.C. Larbalestier, A.W. West, Acta Metall. 32 (1984) 1871–1881.
[2] L.A. Boney, T.C. Willis, D.C. Larbalestier, J. Appl. Phys. 77 (1995) 6377–6387.
[3] B.J. Senkowicz, A. Polyanskii, R.J. Mungall, Y. Zhu, J.E. Giencke, P.M. Voyles, C.B. Eom, E.E. Hellstrom, D.C. Larbalestier, Supercond. Sci. Technol. 20 (2007) 650–657.
[4] H. Kitaguchi, A. Matsumoto, H. Kumakura, T. Doi, H. Yamamoto, K. Saitoh, H. Sosiati, S. Hata, Appl. Phys. Lett. 85 (2004) 2842–2844.
[5] W.E. Yetter, D.A. Thomas, E.J. Kramer, Phil. Mag. B 46 (1982) 523–537.
[6] G. Zerweck, J. Low Temp. Phys. 42 (1981) 1–9.
[7] E.J. Kramer, H.C. Freyhardt, J. Appl. Phys. 51 (1980) 4930–4938.
[8] H. Hilgenkamp, J. Mannhart, Rev. Mod. Phys. 74 (2002) 485–549.
[9] J.H. Durrel, N.A. Rutter, Supercond. Sci. Technol. 22 (2009), 013001.
[10] T. Katase, Y. Ishimaru, A. Tsukamoto, H. Hiramatsu, T. Kamiya, K. Tanabe, H. Hosono, Nat. Commun. 2 (2011) 409.
[11] W.D. Si, C. Zhang, X.Y. Shi, T. Ozaki, J. Jaroszynski, Q. Li, Appl. Phys. Lett. 106 (2015), 032602.
[12] S. Lee, J. Jiang, Y. Zhang, C.W. Bark, J.D. Weiss, C. Tarantini, C.T. Nelson, H.W. Jang, C.M. Folkman, S.H. Baek, A. Polyanskii, D. Abraimov, A. Yamamoto, J.W. Park, X.Q. Pan, E.E. Hellstrom, D.C. Larbalestier, C.B. Eom, Nat. Mater. 9 (2010) 397–402.
[13] T. Katase, T. Katase, H. Hiramatsu, V. Matias, C. Sheehan, Y. Ishimaru, T. Kamiya, K. Tanabe, H. Hosono, Appl. Phys. Lett. 98 (2011), 242510.
[14] S. Ueda, S. Takeda, S. Takano, A. Yamamoto, M. Naito, Appl. Phys. Lett. 99 (2011), 232505.
[15] T. Taen, T. Taen, Y. Nakajima, T. Tamegai, H. Kitamura, Phys. Rev. B 86 (2012), 094527.
[16] H. Lin, C. Yao, X.P. Zhang, C.H. Dong, H.T. Zhang, D.L. Wang, Q.J. Zhang, Y.W. Ma, S. Awaji, K. Watanabe, H.F. Tian, J.Q. Li, Sci. Rep. 4 (2014) 6944.
[17] C. Yao, H. Lin, X.P. Zhang, C.H. Dong, D.L. Wang, Q.J. Zhang, Y.W. Ma, S. Awaji, K. Watanabe, IEEE Trans. Appl. Supercond. 25 (2015), 7300204.
[18] J.D. Weiss, C. Tarantini, J. Jiang, F. Kametani, A.A. Polyanskii, D.C. Larbalestier, E.E. Hellstrom, Nat. Mater. 11 (2012) 682–685.
[19] X.P. Zhang, C. Yao, H. Lin, Y. Cai, Z. Chen, J.Q. Li, C.H. Dong, Q.J. Zhang, D.L. Wang, Y.W. Ma, H. Oguro, S. Awaji, K. Watanabe, Appl. Phys. Lett. 104 (2014), 202601.
[20] N. Ni, M.E. Tillman, J.-Q. Yan, A. Kracher, S.T. Hannahs, S.L. Bud'ko, P.C. Canfield, Phys. Rev. B 78 (2008), 214515.
[21] T. Thersleff, K. Iida, S. Haindl, M. Kidszun, D. Pohl, A. Hartmann, F. Kurth, J. Hänisch, R. Hühne, B. Rellinghaus, L. Schultz, B. Holzapfel, Appl. Phys. Lett. 97 (2010), 022506.
[22] A. Gurevich, E.A. Pashitskii, Phys. Rev. B 57 (1998) 13878–13893.
[23] J.H. Durrell, C.B. Eom, A. Gurevich, E.E. Hellstrom, C. Tarantini, A. Yamamoto, D.C. Larbalestier, Rep. Prog. Phys. 74 (2011) 124511.
[24] S.R. Saha, N.P. Butch, K. Kirshenbaum, Johnpierre Paglione, P.Y. Zavalij, Phys. Rev. Lett. 103 (2009), 037005.
[25] G.F. Chen, Z. Li, G. Li, W.Z. Hu, J. Dong, J. Zhou, X.D. Zhang, P. Zheng, N.L. Wang, J.L. Luo, Chin. Phys. Lett. 25 (2008) 3403–3405.
[26] M.F. Chisholm, S.J. Pennycook, Nature 351 (1991) 47–49.
[27] Y. Zhang, C.T. Nelson, S. Lee, J. Jiang, C.W. Bark, J.D. Weiss, C. Tarantini, C.M. Folkman, S.H. Baek, E.E. Hellstrom, D.C. Larbalestier, C.B. Eom, X.Q. Pan, Appl. Phys. Lett. 98 (2011), 042509.
[28] L. Fernández, B. Holzapfel, F. Schindler, B. de Boer, A. Attenberger, J. Hänisch, L. Schultz, Phys. Rev. B 67 (2003), 052503.
[29] A. Gurevich, E.A. Pashitskii, Phys. Rev. B 57 (1998) 13878–13893.
[30] S. Avci, O. Chmaissem, D.Y. Chung, S. Rosenkranz, E.A. Goremychkin, J.P. Castellan, I.S. Todorov, J.A. Schlueter, H. Claus, A. Daoud-Aladine, D.D. Khalyavin, M.G. Kanatzidis, R. Osborn, Phys. Rev. B 85 (2012), 184507.
[31] M. Yi, D.H. Lu, J.G. Analytis, J.-H. Chu, S.-K. Mo, R.-H. He, R.G. Moore, X.J. Zhou, G.F. Chen, J.L. Luo, N.L. Wang, Z. Hussain, D.J. Singh, I.R. Fisher, Z.-X. Shen, Phys. Rev. B 80 (2009), 024515.
[32] R. Griessen, H.H. Wen, A.J.J. van Dalen, B. Dam, J. Rector, H.G. Schnack, S. Libbrecht, E. Osquiguil, Y. Bruynseraede, Phys. Rev. Lett. 72 (1994) 1910–1913.
[33] D. Dew-Hughes, Phil. Mag. 30 (1974) 293–305.
[34] C.H. Dong, H. Lin, H. Huang, C. Yao, X.P. Zhang, D.L. Wang, Q.J. Zhang, Y.W. Ma, S. Awaji, K. Watanabe, J. Appl. Phys. 119 (2016), 143906.
[35] L. Fang, Y. Jia, J.A. Schlueter, A. Kayani, Z.L. Xiao, H. Claus, U. Welp, A.E. Koshelev, G.W. Crabtree, W.-K. Kwok, Phys. Rev. B 84 (2011), 140504.
[36] R. Prozorov, M.A. Tanatar, N. Ni, A. Kreyssig, S. Nandi, S.L. Bud'ko, A.I. Goldman, P.C. Canfield, Phys. Rev. B 80 (2009), 174517.
[37] A. Gurevich, Supercond. Sci. Technol. 20 (2007) S128–S135.
[38] E.C. Blomberg, M.A. Tanatar, R.M. Fernandes, I.I. Mazin, B. Shen, H.H. Wen, M.D. Johannes, J. Schmalian, R. Prozorov, Sign-reversal of the in-plane resistivity anisotropy in hole-doped iron pnictides, Nat. Commun. 4 (2013) 1914.
[39] B. Xu, Y.M. Dai, H. Xiao, B. Shen, Z.R. Ye, A. Forget, D. Colson, D.L. Feng, H.H. Wen, X.G. Qiu, R.P.S.M. Lobo, Optical observation of spin-density-wave fluctuations in Ba122 iron-based superconductors, Phys. Rev. B 94 (2016), 085147.